Title

Conductive Polymer Binder for High-Tap-Density Nanosilicon Material for Lithium-Ion Battery Negative Electrode Application

Journal

Nano Letters, 15(12)

ISSN

1530-6984

Authors

Zhao, Hui

Wei, Yang

Qiao, Ruimin

et al.

Publication Date

2015-12-09

DOI

10.1021/acs.nanolett.5b03003

Peer reviewed

Conductive polymer binder for high-tap-density nano-silicon material for lithium-ion battery negative electrode application

Hui Zhao,[a] Yang Wei,[b] Ruimin Qiao,[c] Chenhui Zhu,[c] Ziyan Zheng,[a] Min Ling,[a] Zhe Jia,[a] Ying Bai,[a,d] Yanbao Fu,[a] Jinglei Lei,[a,e] Xiangyun Song,[a] Vincent S. Battaglia,[a] Wanli Yang,[c] Phillip B. Messersmith,[b] and Gao Liu[a*]

[a]*Energy Storage and Distributed Resources Division, Energy Technologies Area,* [c]*Advanced Light Source, Lawrence Berkeley National Laboratory, Berkeley, California, 94720, United States*

[b]*Departments of Bioengineering and Materials Science and Engineering, UC Berkeley, California, 94720, United States*

[d]*Beijing Key Laboratory of Environmental Science and Engineering, School of Material Science and Engineering, Beijing Institute of Technology, Beijing 100081, China*

[e]*Chongqing University, Chongqing, 400044, China*

[*] Tel.: +1-510-486-7207; fax: +1-510-486-7303; Email: gliu@lbl.gov (G. Liu)

Abstract: High-tap-density silicon nanomaterials are highly desirable as anodes for lithium ion batteries, due to their small surface area and minimum first-cycle loss. However, this material poses formidable challenges to polymeric binder design. Binders adhere on to the small surface area to sustain the drastic volume changes during cycling; also the low porosities and small pore size resulting from this material are detrimental to lithium ion transport. This study introduces a new binder, Poly(1-pyrenemethyl methacrylate-co-methacrylic acid) (PPyMAA), for a high-tap-density nano-silicon electrode cycled in a stable manner with a first cycle efficiency of 82% - a value that is further improved to 87% when combined with graphite material. Incorporating the MAA acid functionalities does not change the lowest unoccupied molecular orbital (LUMO) features or lower the adhesion performance of the PPy homopolymer. Our single-molecule force microscopy measurement of PPyMAA reveals similar adhesion strength

between polymer binder and anode surface when compared with conventional polymer such as homo-polyacrylic acid (PAA), while being electronically conductive. The combined conductivity and adhesion afforded by the MAA and pyrene copolymer results in good cycling performance for the high-tap-density Si electrode.

Keywords: conductive polymer binder, single molecule force, silicon nanoparticle, high tap density, lithium-ion battery

Introduction

State-of-the-art lithium-ion batteries use graphite as an anode, with a theoretical gravimetric specific capacity of 372 mAh/g. Alternative alloy anode materials such as tin (Sn, 994 mAh/g) and silicon (Si, 4200 mAh/g) have much higher gravimetric specific capacities;[1] however, almost 300% volume expansion occurs as the material transitions from Si to its fully lithiated phase.[2] Because of this large volume change, the electronic integrity of the composite electrode is disrupted in addition to extensive and continuous surface side reactions are induced, leading to a drastic capacity decay.[3] Among various efforts to address this challenge, nanostructured active materials are most promising because of their ability to alleviate mechanical strain induced by volume change. Different forms of Si nano-structures, such as nanowires,[4,5] nanotubes,[6] and thin films[7] have been largely explored. However, the high surface area of the nano-architecture leads to excessive solid electrolyte interphase (SEI) growth, causing very low first cycle efficiencies (typically in the range of 60% to 70%) compared to the high first cycle efficiency of graphite (85% to 90%).[8]

The work described in this paper focuses on a commercial high-tap-density nanoSi material with a uniform size distribution of around 200 nm. The absence of fused, branched particles and very small particles results in a nanoSi material of high tap-density and a low available surface area for adhesion of polymer binders; consequently SEI growth in the initial cycles is reduced to a minimum.

Results of this work demonstrate that a good polymeric binder is also an effective way to obtain stable electrochemical performance.[9] Traditionally, the following categories of binders are shown as being effective for Si anode: natural polymer like carboxymethyl cellulose (CMC) and

alginate, conventional synthetic polymer such as polyacrylic acid (PAA) and polyimide, and conductive polymer binders among others.[9] Adopted from the ideas of PAA and conductive polymer binders, a multifunctional conductive polymer binder is designed in this study to adapt to the nano-Si anode on the molecular level, leading to highly stable electrochemical performance.

Results and Discussion

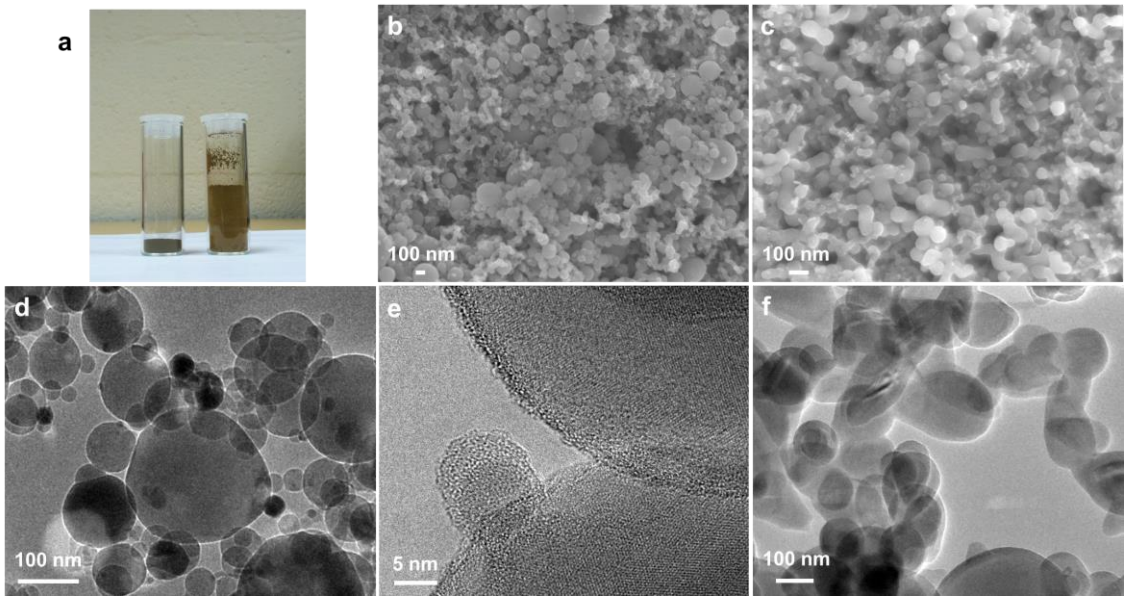

Figure 1. (a) A comparison of 0.3 g of high-tap-density nanoSi (left) and regular nanoSi produced by chemical vapor deposition (right). Scanning electron microscopy (SEM) images of (b) high tap-density nanoSi and (c) regular nanoSi. Transmission electron microscopy (TEM) images of (d) (e) high tap-density nanoSi and (f) regular nanoSi.

Comparison between high-tap-density nanoSi and a regular nanoSi. Figure 1a shows the same type of vials with 0.3 g of high-tap-density nanoSi (left) and regular nanoSi (right). It is apparent that the high-tap-density nanoSi has high packing density compared to the regular nanoSi. The regular nanoSi shown here was synthesized using a chemical vapor deposition (CVD) process, which has an average particle size of 50-70 nm and a tap density of 0.1 g/cm^3. Most of the particles are fused together in the regular nanoSi (Figure 1c, f); the fused particles form a "network"-like structure that is maintained even after the laminate fabrication. Thus, the high surface area of the pristine CVD nanoSi translates into a high porosity of the electrode laminate,

which has a typical calculated pore value of 86%. SEM indicates that the high tap-density nanoSi has a regular round shape with a median size of 200 nm (Figure 1b, d). Although this Si particle is in nano-size, Brunarer-Emmett-Teller (BET) analysis indicates a surface area of only 12 m^2/g, with a tap-density of 0.51 g/cm^3. Note that this commercial nanoSi has a tap density that is comparable with some specially-designed high tap-density nanoSi reported in the literature.[10] The round-shaped and non-fused high tap-density nanoSi is easily condensed during slurry preparation and laminate fabrication, producing an electrode with smaller porosity of ~ 79%. With a high tap density and lower surface area, this Si anode intrinsically needs less SEI formation to passivate the anode surface, which could potentially lead to a high first-cycle coulombic efficiency. A very thin surface oxide layer is shown in the high resolution TEM image (Figure 1e), translating into less side reaction and smaller impedance,[11,12] but still providing a surface functionality for binder adhesion.[13] The crystalline Si phase is detected in TEM, consistent with the x-ray diffraction analysis in Supporting Figure S1.

	High tap-density nanoSi	Regular nanoSi
Particle morphology	Well-defined round shaped particles, easily condensed after electrode laminate	particles fused together even after electrode laminate
Particle size	~200 nm	50 nm
Tap density	0.51 g/cm^3	0.10 g/cm^3
BET Surface area	12 m^2/g	55 m^2/g
Electrode porosity (10% PPyMAA)	79%	86%
First cycle efficiency (at C/10 rate)	82.08%	74.39%

Table 1. The key parameters of high tap-density nanoSi and regular nanoSi.

The surface area of the nanoSi and electrode porosities have a direct influence on the electrochemical performance, especially on the coulombic efficiency (CE) at first cycle. High

surface area needs more SEI to passivate the whole electrode surface, which typically causes large irreversible capacities in the first cycle. As shown in Table 1, an electrode with normal nanoSi has a first cycle CE of only 74%, while this value for an electrode with high tap-density is typically around 82%. The low first cycle CE associated with most nanoSi is a challenge when assembling a lithium ion cell, since the expensive lithium source in the cathode is consumed. The use of the high tap-density nanoSi shown in this work represents a very promising solution.

Design and characterization of the conductive polymer binder for high-tap-density nanoSi. When assembling a lithium-ion electrode with high-tap-density nanoSi, the lower surface area poses formidable challenges to prevent particle isolation and electrode failure resulting from drastic volume changes when cycling the cell. The low-cost, versatile synthetic route to a pyrene-based side chain conductive polymer binder opens up new possibilities in binders and electrode design. Pyrene-based polymers were established as a class of electric conductive polymeric binders that can maintain the electrode mechanical integrity and Si interface stability over long term cycling.[14]

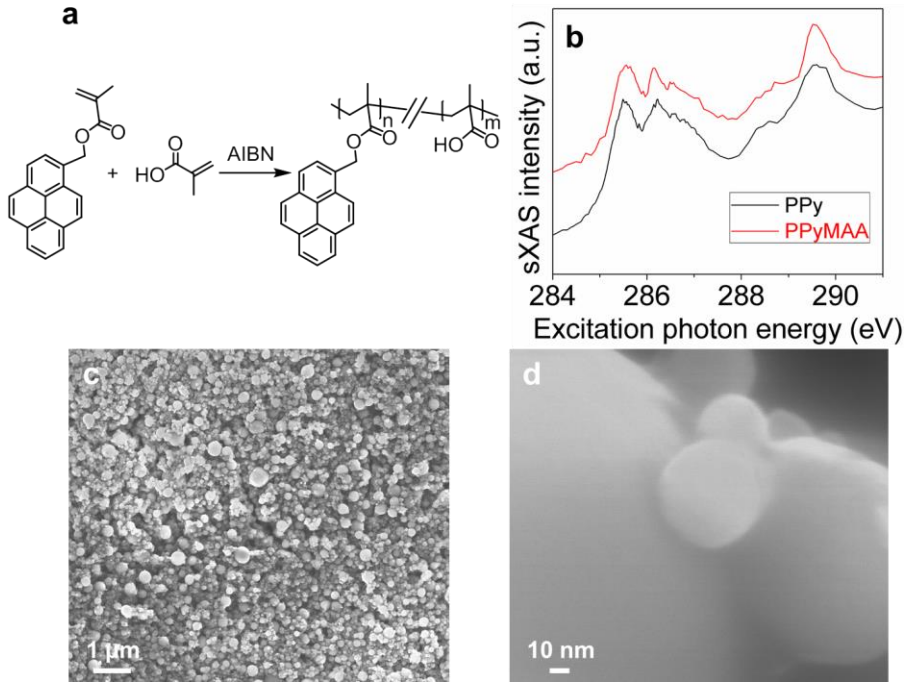

Figure 2. (a) The generic synthesis of PPyMAA polymer binder. (b) Carbon K-edge sXAS of PPy and PPyMAA shows that the LUMO energy is intact in PPyMAA, although non-conductive methacrylic acid groups are introduced. (c) and (d) SEM images of the PPyMAA/high-tap density nanoSi electrode.

In addition to electronic conductivity, adhesion between binder and active Si particles is important to prevent particle isolation and allow the particles to endure drastic volume changes during cycling. To accommodate volume changes and take full advantage of the small surface area of the high tap-density nanoSi, a methacrylic acid (MAA) monomer was copolymerized with the 1-pyrenemethyl methacrylate in a free-radical polymerization process, initiated by 2, 2′-azobis (2-methylpropionitrile) (AIBN), as shown in Figure 2a. A random copolymer, poly(1-pyrenemethyl methacrylate-co-methacrylic acid) (PPyMAA) is obtained, containing an electric-conducting pyrene moiety and the acid units for better adhesion. The hydrogen bonding between carboxylic acid groups in PAA and CMC with the silanol surface group on Si particles enables the particles to accommodation textural stresses evolved during cycling, which proves to be critical for the satisfactory performance of Si-based electrodes. Furthermore, the covalent bonding between the binder and the Si materials has been experimentally confirmed.[15] It is

proposed that the MAA structures incorporated into this binder performs similar functions; the binder is then able to minimize surface area in the high-tap-density nanoSi.

The content of MAA is limited to 30 mol% to enhance the adhesion of the binder while not disturbing the conjugation of the PPy unit. Wide angle X-ray scattering (WAXS) of the PPy and PPyMAA polymers exhibit very similar pattern (Figure S5), indicating that the ordered phase characteristic of the pyrene is still maintained in the synthesized PPyMAA copolymer. To ensure that the newly-designed PPyMAA binder still maintains the electronic conductivity, the study looked at the electronic structure of both the PPy and PPyMAA polymers using synchrotron-based x-ray absorption spectroscopy (sXAS). sXAS is a direct probe of the excitations of core level electrons to the unoccupied valence states. Previous results of this work demonstrated that sXAS could be employed to study the electric properties of polymer materials efficiently.[16,17] The methodology is based on the fact that the lowest-energy sXAS feature directly corresponds to the state of the lowest unoccupied molecular orbital (LUMO), which is very sensitive to the electric properties of the polymers.[18] Figure 2b shows the sXAS spectra of PPy and PPyMAA. The splitting peaks around 285-286 eV correspond to the $\pi^*_{C=C}$ bonds with conjugation, and the features around 288 eV are from $\pi^*_{C=O}$.[18] The study focused on the low-energy sXAS features corresponding to the LUMO states. It is obvious that incorporating the MAA group does not change the lowest-energy features in sXAS, indicating the LUMO of the PPy polymer is intact in PPyMAA. The consistency of the overall lineshape also implies that the electron states close to the Fermi level are dominated by the pyrene-based PPy states. This comparison is thus reliable without core-hole potential concerns.[16]

The synthesized PPyMAA polymer was used as a binder to assemble electrode laminate with high-tap-density nanoSi, with a composition of 10% binder and 90% nanoSi. The morphology of the electrode is shown in Figure 2c and 2d. A good porosity is exhibited in this electrode morphology, which is necessary for a good lithium ion transport. Polymer binder uniformly coated on the nanoSi particle surface (Figure 2d), which provides good particle/particle cohesion.

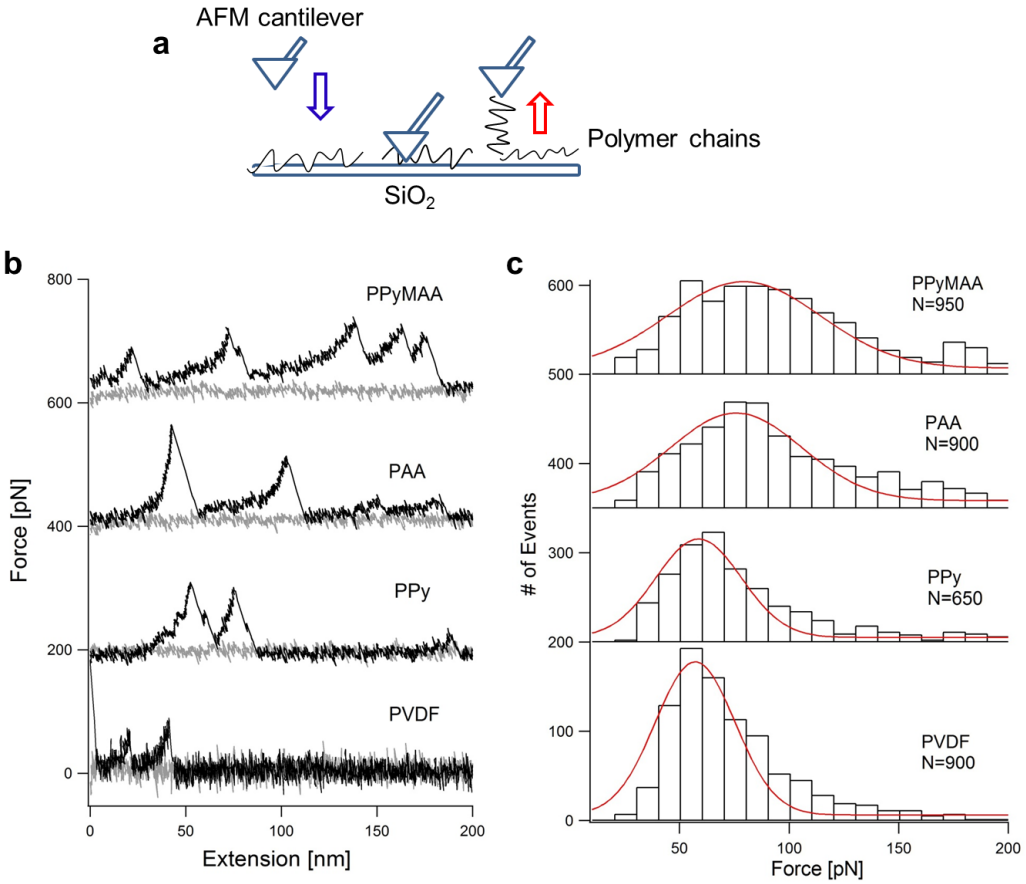

Figure 3. (a) A schematic description of the single-molecule AFM experiment. (b) AFM force-extension curves representing pulling polymer binders from glass surface in 1M LiCl, pH 6.7. Force curves are displaced vertically for display purposes. (c) Histograms of AFM rupture force distribution corresponding to pulling a single polymer chain from a glass surface. Averaged rupture forces for PPyMAA, PAA, PPy, and PVDF on glass substrate were 95±58, 99±54, 72±40 and 68±38 piconewton (pN), respectively, with mean rupture forces ± standard deviations and N= # of observed unbinding events. The pulling velocity is 1000 nm/s and dwell time is 0.5 seconds.

Unbinding force of pulling a single binder on a glass substrate. Since the performance of a polymer binder in an anode is expected to depend on adhesion strength between the electrode and polymer binders, experimental studies in this section investigate the unbinding forces

originating from pulling a single polymer chain of different binders from glass substrate (Figure 3a), with the understanding that the high unbinding force of a single attached polymer chain correlates to strong affinity to the substrate. The typical force-extension curves of each polymer are shown in Figure 3b. To ensure that the observed forces originated from a single molecular event, a novel screening protocol for rejecting the unbinding force arising from multiple chains was employed and is described in detail in Figure S6 in supporting information. Figure 3c shows the histogram of unbinding events of pulling a single chain of PVDF, PPy, PAA, and PPyMAA binders from glass substrate at a constant speed. As shown, the unbinding force histogram of PPy agrees well with the most conventional but poor Si anode binders such as PVDF, with both polymer binders attached to the glass substrate primarily through van der Waals forces, which lead to a tight shape of rupture force distribution and usually fails to ensure the integrity of the anode.[19] On the other hand, the unbinding force histograms of both PAA and PPyMAA on glass surfaces exhibiting similar shape in distributions are substantially wider than that of conventional PVDF binder on glass, reflecting an additional attraction considered to be provided by hydrogen bonds.[20] As a result, when compared with PAA, the PPyMAA copolymer with 70 mol% pyrene and 30 mol% MAA structure could be considered as effective Si anode binder based on our AFM force results, contributing acceptable adhesion while maintaining better electronic structure for *in-situ* doping in the lithium ion battery anode operational voltage.

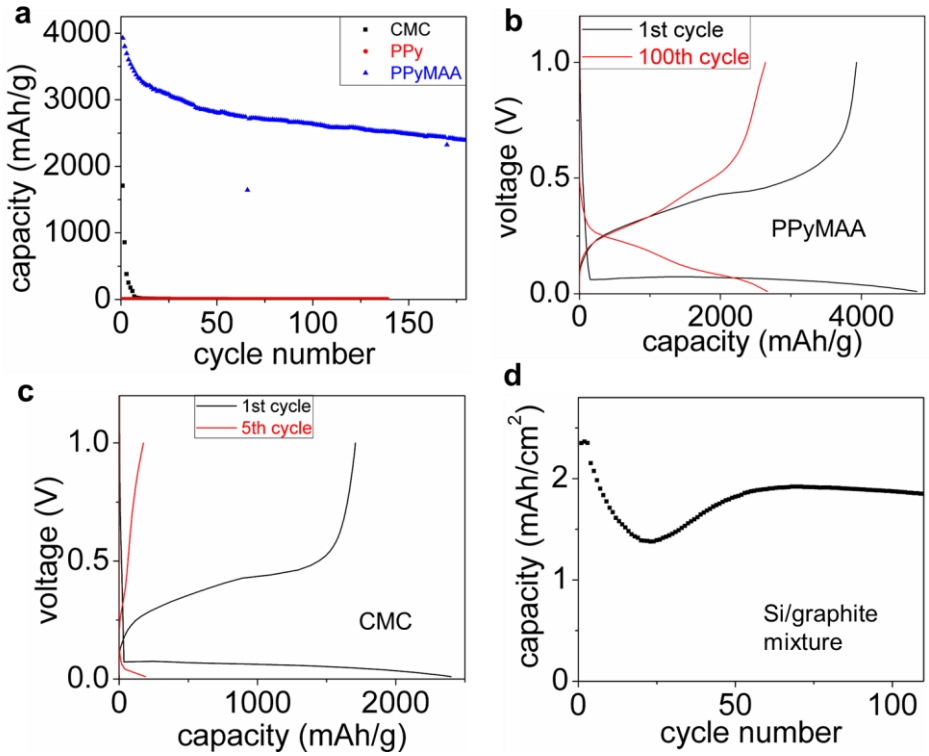

Figure 4. (a) Charge (delithiation) capacities of high tap density Si electrodes at C/10 with different binders. (b) The 1st and 100th cycle voltage curves of the PPyMAA/Si cell. (c) The 1st and 5th cycle voltage curves of the CMC/Si cell. (d) Charge (delithiation) capacities of the Si/graphite mixture electrodes with PPyMAA binder at C/10. The electrode is composed of 10% binder, 10% high tap density nanoSi and 80% graphite.

Electrochemical performance of the high tap-density nanoSi with PPyMAA. Figure 4a shows the galvanostatic cycling performance of high tap-density nanoSi with a lithium metal counter electrode at a C/10 (420 mA/g) rate. For all three binders, the compositions of the electrodes are 10 wt% binder with 90 wt% nanoSi. The nanoSi/PPyMAA electrode maintains a reversible capacity of 2200 mAh/g for over 180 cycles. PPy binder without the acid functional group, on the other hand, directly leads to cell failure of the nano-Si anode (Figure 4a), as well as CMC, PVDF, and PAA (Figure S3). The voltage curves of PPyMAA and CMC cells are shown in Figure 4b and 4c. A large crystalline phase is detected in the TEM morphology of the nanoSi (Figure S4), and a large overpotential is shown in the first cycle lithiation curve, corresponding to the crystalline Si phase to the amorphous phase transition.[21] A reversible capacity of 2800 mAh/g is shown in the

100^{th} cycle when using PPyMAA binder, whereas the CMC-based cell exhibits failure in only the fifth cycle.

As the most promising anode material for next-generation lithium-ion batteries, silicon material is mixed as a small portion of the anode together with graphite. The electrode is composed of 10% PPyMAA binder, 10% high-tap-density nanoSi, and 80% graphite. To assemble a relatively high-loading cell using the nanoSi and to confirm the compatibility with the application of the common graphite anode, graphite is mixed when preparing the slurry and electrode laminate. An initial dip of the capacity values is shown in the nanoSi/graphite cell, presumably due to the slow wetting of the electrolyte on the thick electrode. After 50 cycles, a stable areal capacity of 2 mAh/cm^2 is shown in Figure 4d.

		nanoSi/PPyMAA	nanoSi/CMC	nanoSi/graphite/PPyMAA
1^{st} cycle	Q_c[a](mAh/g)	3928.8	1708.5	579.3
	η[b] (%)	82.08	71.18	87.05
5^{th} cycle	Q_c[a] (mAh/g)	3536.7	175.5	511.5
	η[b] (%)	97.27	92.49	98.49
100^{th} cycle	Q_c[a] (mAh/g)	2638.1	2.4	461.9
	η[b] (%)	98.94	X	99.52

[a] charge (delithiation) capacity [b] Coulombic efficiency

Table 2. Electrochemical parameters of high tap-density nanoSi electrodes.

The key electrochemical parameters of the nanoSi cell are shown in Table 2. A typical first cycle efficiency of 82% is shown for the high-tap-density nanoSi/PPyMAA cell, which is further improved when mixing with graphite, yielding a value of 87%. Combining electronic conductivity (Py) with interfacial adhesion (MAA), the copolymer enables a high specific capacity (delithiation) of almost 4000 mAh/g in the initial several cycles. Drastic volume changes are associated with this high specific capacity, which eventually stabilize at around 2500 mAh/g and lasts for more than 200 cycles. In contrast, CMC binder only delivers a delithiation capacity of 1700 mAh/g in even the first cycle, and cell failure occurs after only several cycles. The comparison of the

electrochemical parameters shown in Table 2 further showcases the advantage of the bi-functional PPyMAA binder for use in high-tap-density nanoSi anodes.

Conclusions

High tap density nanoSi is a desirable anode candidate to eliminate the typically high irreversible capacities for silicon nano--materials, yet the small surface area poses formidable challenges to the design of applicable polymeric binders. A multifunctional conductive polymer binder with both electronic conductivity and adhesion functionalities is synthesized and used for a high tap density nanoSi anode. AFM based single molecule force measurements confirms that the material can bind to nanoSi with similar affinity to other effective Si anode binders such as PAA binder, while being more conductive due to the presence of pyrene in the copolymer structure. A long-term stable cycling performance is obtained for the multifunctional conductive polymer binder/nanoSi anode with high first cycle coulombic efficiency. The high tap-density nanoSi-based high capacity anodes enabled by the PPyMAA binder shows great promise toward a commercial product.

ASSOCIATED CONTENT

Supplementary Information

Details about polymer synthesis, battery assembly and testing, single-molecule force data. This material is available free of charge via the Internet at http://pubs.acs.org

AUTHOR INFORMATION

Corresponding Author

*E-mail: gliu@lbl.gov

Notes

The authors declare no competing financial interests.

ACKNOWLEDGEMENTS

This work was funded by the Assistant Secretary for Energy Efficiency, Vehicle Technologies Office of the U.S. Department of Energy (U.S. DOE) under the Advanced Battery Materials

Research (BMR) and Applied Battery Research (ABR) Programs, supported by the U.S. Department of Energy under Contract # DE-AC02-05 CH11231. Soft X-ray absorption measurement and analysis at the Advanced Light Source (ALS), and nuclear magnetic resonance spectroscopy (NMR) analyses at the Molecular Foundry—all located at Lawrence Berkeley National Laboratory and supported by the Director, Office of Science, Office of Basic Energy Sciences, of the U.S. Department of Energy. The authors acknowledge support of the National Center for Electron Microscopy, Lawrence Berkeley Lab, which is supported by the U.S. Department of Energy under Contract # DE-AC02-05 CH11231. Ruimin Qiao is supported by the LDRD program at the Lawrence Berkeley National Laboratory. The authors acknowledge partial support from NIH grant R37 DE014193.

References

1. Boukamp, B. A.; Lesh, G. C.; Huggins, R. A. *J. Electrochem. Soc.* **1981,** 128, (4), 725-729.

2. Li, J.; Dahn, J. R. *J. Electrochem. Soc.***2007,** 154, (3), A156-A161.

3. Ryu, J. H.; Kim, J. W.; Sung, Y.-E.; Oh, S. M. *Electrochem. Solid-State Lett.* **2004,** 7, (10), A306-A309.

4. Deshpande, R.; Cheng, Y.-T.; Verbrugge, M. W. *J. Power Sources* **2010,** 195, (15), 5081-5088.

5. Park, M.-H.; Kim, M. G.; Joo, J.; Kim, K.; Kim, J.; Ahn, S.; Cui, Y.; Cho, J. *Nano Lett.* **2009,** 9, (11), 3844-3847.

6. Yoo, J.-K.; Kim, J.; Jung, Y. S.; Kang, K. *Adv. Mater.* **2012,** 24, (40), 5452-5456.

7. He, Y.; Yu, X.; Wang, Y.; Li, H.; Huang, X. *Adv. Mater.* **2011,** 23, (42), 4938-4941.

8. Wu, H.; Cui, Y. *Nano Today* **2012,** 7, (5), 414-429.

9. Zhao, H.; Yuan, W.; Liu, G. *Nano Today* **2015,** 10, (2), 193-212.

10. Liu, N.; Lu, Z.; Zhao, J.; McDowell, M. T.; Lee, H.-W.; Zhao, W.; Cui, Y. *Nat. Nanotech.* **2014,** 9, 187–192.

11. Xun, S.; Song, X.; Grass, M. E.; Roseguo, D. K.; Liu, Z.; Battaglia, V. S.; Liu, G.

Electrochem. Solid-State Lett. **2011,** 14, (5), A61-A63.

12. Xun, S.; Song, X.; Wang, L.; Grass, M. E.; Liu, Z.; Battaglia, V. S.; Liu, G. *J. Electrochem. Soc*. **2011,** 158, (12), A1260-A1266.

13. Hochgatterer, N. S.; Schweiger, M. R.; Koller, S.; Raimann, P. R.; Wöhrle, T.; Wurm, C.; Winter, M. *Electrochem. Solid-State Lett.* **2008,** 11, (5), A76-A80.

14. Park, S.-J.; Zhao, H.; Ai, G.; Wang, C.; Song, X.; Yuca, N.; Battaglia, V. S.; Yang, W.; Liu, G. *J. Am. Chem. Soc.* **2015**.

15. Zhao, H.; Wang, Z.; Lu, P.; Jiang, M.; Shi, F.; Song, X.; Zheng, Z.; Zhou, X.; Fu, Y.; Abdelbast, G.; Xiao, X.; Liu, Z.; Battaglia, V. S.; Zaghib, K.; Liu, G. *Nano Lett.* **2014,** 14, (11), 6704-6710.

16. Liu, G.; Xun, S. D.; Vukmirovic, N.; Song, X. Y.; Olalde-Velasco, P.; Zheng, H. H.; Battaglia, V. S.; Wang, L. W.; Yang, W. L. *Adv. Mater.***2011,** 23, (40), 4679-4683.

17. Wu, M.; Xiao, X.; Vukmirovic, N.; Xun, S.; Das, P. K.; Song, X.; Olalde-Velasco, P.; Wang, D.; Weber, A. Z.; Wang, L.-W.; Battaglia, V. S.; Yang, W.; Liu, G. *J. Am. Chem. Soc.* **2013,** 135, (32), 12048-12056.

18. Stohr, J., *NEXAFS Spectroscopy*. Springer Science & Business Media: 1992.

19. Magasinski, A.; Zdyrko, B.; Kovalenko, I.; Hertzberg, B.; Burtovyy, R.; Huebner, C. F.; Fuller, T. F.; Luzinov, I.; Yushin, G. *ACS Appl. Mater. Interfaces* **2010,** 2, (11), 3004-3010.

20. Song, J.; Zhou, M.; Yi, R.; Xu, T.; Gordin, M. L.; Tang, D.; Yu, Z.; Regula, M.; Wang, D. *Adv. Funct. Mater.* **2014,** 24, (37), 5904-5910.

21. Key, B.; Morcrette, M.; Tarascon, J.-M.; Grey, C. P. *J. Am. Chem. Soc.* **2011,** 133, (3), 503-512.

TOC